

Meta Distribution of Partial-NOMA

Konpal Shaukat Ali, *Member, IEEE*, Arafat Al-Dweik, *Senior Member, IEEE*, Ekram Hossain, *Fellow, IEEE*, and Marwa Chafii, *Member, IEEE*

Abstract—This work studies the meta distribution (MD) in a two-user partial non-orthogonal multiple access (pNOMA) network. Compared to NOMA where users fully share a resource element, pNOMA allows sharing only a fraction α of the resource element. The MD is computed via moment-matching using the first two moments where reduced integral expressions are derived. Accurate approximates are also proposed for the b th moment for mathematical tractability. We show that in terms of percentile-performance of links, pNOMA only outperforms NOMA when α is small. Additionally, pNOMA improves the percentile-performance of the weak-user more than the strong-user highlighting its role in improving fairness.

Index Terms: Non-orthogonal multiple access (NOMA), stochastic geometry, meta distribution.

I. INTRODUCTION

While non-orthogonal multiple access (NOMA) enables a complete sharing of the resource element (RE) by multiple user equipment (UE) to improve throughput, the introduced intracell interference (IaCI) deteriorates the UE coverage. On the contrary, orthogonal multiple access (OMA) has no IaCI, which results in superior coverage, but no spectrum reuse can be applied, which hinders the throughput. Therefore, partial non-orthogonal multiple access (pNOMA) is introduced as a compromise between OMA and NOMA [1]. In contrast to NOMA, UEs in pNOMA share only a fraction α of the RE, which allows spectrum reuse while limiting the IaCI encountered by UEs. In [1], partial sharing of an RE by two users is accomplished by having the two signals overlap only with a fraction of each other in the frequency domain while having complete access to the entire time slot. The partial overlap in the frequency domain allows using matched filtering at the receiver side to further suppress the interference encountered by the UEs, resulting in improved coverage. The matched filtering also enables devising a new decoding technique referred to as flexible successive interference cancellation (FSIC). Using matched filtering in conjunction with FSIC allows pNOMA to outperform NOMA in terms of throughput [1].

Stochastic geometry provides a unified mathematical paradigm for modeling large wireless networks and characterizing their operation while taking into account the experienced intercell interference (ICI) [2], [3]. Research on NOMA [4]–[11] and pNOMA

[1] have used these tools to analyze networks that encounter both IaCI and ICI. Stochastic geometry-based studies of networks often focus on the spatial averages of performance metrics, the most frequent being the averaged spatial coverage probability (SCP), which averages performance overall fading, activity, and network realizations. However, the actual performance distribution of the majority of the links may not necessarily be close to the SCP. Spatial averages thus do not reveal information about the percentile performance of links that the network operators would be interested in as these reveal the quality of service that the network can offer. It is thus pertinent to study the percentile performance of UEs, where the fading and activity change while the network realization is kept constant. The coverage probability given a fixed network realization is defined as the conditional coverage probability (CCP) [12]. The complementary cumulative distribution function (CCDF) of the CCP, denoted as the meta distribution (MD), reveals the percentile performance across an arbitrary network realization. Since the MD can only be obtained numerically using the Gil-Pelaez theorem, the beta distribution using moment matching of the first two moments of the CCP was proposed as an accurate approximation of the MD [12]. Works such as [9]–[11], have studied the MD for NOMA UEs using this approach.

The SCP, which is the 1st moment of the CCP, is studied in [1] for a two-user pNOMA network. In contrast, this work focuses on studying the MD of UEs in such a network to reveal more fine-grained information about the performance of such a setup. We derive integral expressions for the b th moment of the CCP in a pNOMA network. For the first two moments, which are required to approximate the MD via moment matching, we are able to reduce the integrations required. We also propose accurate approximations for the b th moment of the CCP to further simplify the integral calculation and reveal performance trends. Using the exact and approximate moments of the CCP, we compute the MD. This reveals fine-grained information such as the 5%-user performance, which is the reliability that 95% of the UEs can achieve. Our results highlight the superiority of the percentile performance of pNOMA over traditional NOMA in the low α regime. Further, we show that pNOMA improves the performance of the weak UE more, highlighting its role in improving fairness.

Notation: We denote vectors using bold text, $\|\mathbf{z}\|$ is used to denote the Euclidean norm of the vector \mathbf{z} and $b(\mathbf{z}, R)$ denotes a ball centered at \mathbf{z} with radius R . The indicator function, denoted as $\mathbb{1}_A$ has value 1 when event A occurs and is 0 otherwise. We use $\psi(x) = \sin(\pi x)/(\pi x)$ when $x \neq 0$, and $\psi(x) = 1$ when $x = 0$. $\mathbb{E}[\cdot]$ is the expectation and the probability of A is denoted as $\mathbb{P}(A)$.

K. S. Ali and M. Chafii are with the Engineering Division, New York University (NYU) Abu Dhabi, 129188, UAE. (Email: {konpal.ali, marwa.chafii}@nyu.edu). M. Chafii is also with NYU WIRELESS, NYU Tandon School of Engineering, Brooklyn, 11201, NY.

A. Al-Dweik is with the Center for Cyber-Physical Systems (C2PS), Department of Electrical Engineering and Computer Science, Khalifa University, Abu Dhabi, P.O.Box 127799, UAE. (Email: arafat.dweik@ku.ac.ae, dweik@fulbrightmail.org).

E. Hossain is with the Department of Electrical and Computer Engineering, University of Manitoba, Winnipeg, Canada (Email: ekram.hossain@umanitoba.ca).

This work was supported in part by the Technology Innovation Institute (TII), Abu Dhabi, UAE, Grant. no. GC/090-20.

II. SYSTEM MODEL AND ASSUMPTIONS

A. Network Model

We consider a downlink cellular network where the base stations (BSs) are distributed according to a homogeneous Poisson point process (PPP) Φ with intensity λ . As a large network is being studied, we assume an interference-limited regime. A BS serves two UEs in each RE via pNOMA using a total power budget of $P = 1$. Note that, for simplicity, we do not study pNOMA for more than two UEs sharing a RE as such a setup complicates the analysis without providing additional insights. To the network, we add a BS at the origin \mathbf{o} , which under expectation over Φ , becomes the typical BS serving UEs in the typical cell. We study the performance of the typical cell over one RE. As Φ does not include the BS at \mathbf{o} , the set of interfering BSs for the UEs in the typical cell is denoted by Φ . The distance between the typical BS at \mathbf{o} and its nearest neighboring BS is denoted by ρ . Since Φ is a PPP, the probability density function (PDF) of ρ is $f_\rho(x) = 2\pi\lambda x e^{-\pi\lambda x^2}$, $x \geq 0$.

Consider a disk around the BS at \mathbf{o} with radius $\rho/2$, i.e., $b(\mathbf{o}, \rho/2)$, this is referred to as the in-disk [1], [4], [9]. The in-disk is the largest disk centered at a BS that fits inside its Voronoi cell. Two pNOMA UEs are distributed uniformly and independently at random in the in-disk $b(\mathbf{o}, \rho/2)$ of the BS at \mathbf{o} . The rationale behind using such a model where UEs are not too far from the serving BS in setups where each UE does not have an individual dedicated RE was shown in [9]. A Rayleigh fading environment is assumed where the fading coefficients are independent and identically distributed (iid) with a unit-mean exponential distribution. A power-law path-loss model is considered where the signal decays at the rate $r^{-\eta}$ with distance r , $\eta > 2$ denotes the path-loss exponent and $\frac{2}{\eta} \triangleq \delta$. Fixed-rate transmissions are used by the BSs.

B. pNOMA Model

A BS serves two UEs in each RE via pNOMA by multiplexing the signals for each UE with different power levels using the total power P . The RE is split into three regions [1, Fig. 1], \mathfrak{R}_1 , \mathfrak{R}_2 and \mathfrak{R}_3 , where \mathfrak{R}_2 is shared by the two UEs. The fraction of the bandwidth (BW) in \mathfrak{R}_2 is α ; thus, the UEs have full access to the time slot while they share an overlap α of the frequency. We refer to the fraction of the BW in region \mathfrak{R}_1 , accessible to only UE₁, by β , where $0 \leq \beta \leq 1 - \alpha$. The remaining fraction of the BW, $1 - \alpha - \beta$, in region \mathfrak{R}_3 , is available solely to UE₂. Thus, the total fraction of the BW available to UE₁ (UE₂) is $\text{BW}_1 = \alpha + \beta$ ($\text{BW}_2 = 1 - \beta$).

An overlap in the frequency domain allows implementing filtering at the receiver side to further suppress interference. A matched filter that has a Fourier transform equal to the complex conjugate of the Fourier transform of the transmitted signal is used [1], [13]. In this work, we adopt square pulse shaping for transmissions of both UEs. A message that goes through receive filtering and has an α -overlap with the message of the UE of interest will be scaled by an effective interference factor $0 \leq \mathcal{I}(\alpha, \beta) \leq 1$. From [1], the effective interference factor as a function of β and the overlap α is calculated as

$$\mathcal{I}(\alpha, \beta) = \left(\int_{\beta}^{\beta+\alpha} \frac{1}{E_1 E_2} \psi\left(\frac{f-f_a}{0.5\text{BW}_1}\right) \psi\left(\frac{f-f_b}{0.5\text{BW}_2}\right) df \right)^2 \quad (1)$$

where the center frequency of UE₁ is $f_a = \frac{\alpha+\beta}{2}$ and UE₂ is $f_b = \frac{1+\beta}{2}$. The factors E_i for $i \in \{1, 2\}$ are used to scale the

energy to 1 and are calculated as $E_i^2 = \int_{-\text{BW}_i/2}^{\text{BW}_i/2} \psi^2\left(\frac{2f}{\text{BW}_i}\right) df$. Note that $\mathcal{I}(\alpha, \beta)$ increases monotonically with α and is 1 (0) when $\alpha = 1$ ($\alpha = 0$) [1, Fig. 2]. As $0 \leq \mathcal{I}(\alpha, \beta) \leq 1$, matched filtering results in suppression of the interference from the other UE partially sharing the RE. Since any message that has an α -overlap with the UE of interest is scaled by $\mathcal{I}(\alpha, \beta)$, not only does matched filtering suppress ICI, but also reduces ICI.

We order the UEs based on the link distance R between the typical BS at \mathbf{o} and its UEs that are uniformly distributed in the in-disk with radius ρ . This is equivalent to ordering based on the decreasing received mean signal power, i.e., $R^{-\eta}$. Thus, we refer to the strong (weak) UE as UE₁ (UE₂). As the order of the UEs is known at the BS, we use ordered statistics for the PDF of R_i [14],

$$f_{R_i|\rho}(r | \rho) = 16r\rho^{-2} (4r^2\rho^{-2})^{i-1} (1 - 4r^2\rho^{-2})^{2-i}. \quad (2)$$

While NOMA uses successive interference cancellation (SIC) for decoding, after matched filtering in pNOMA, the message of UE₂ scaled by $\mathcal{I}(\alpha, \beta)$ can be too weak for UE₁ to decode; FSIC was thus introduced in [1] to combat this problem.

The power allocated to UE₁ (UE₂) is denoted by P_1 (P_2) and $P_1 + P_2 = 1$. For fixed rate transmission, the rate of UE _{i} , $i \in \{1, 2\}$, is $\log(1 + \theta_i)$. Accordingly, to decode the message of UE _{i} , the signal to interference ratio (SIR) needs to exceed θ_i . The throughput of UE _{i} , $i \in \{1, 2\}$ is defined as $\mathcal{T}_i = \text{BW}_i \mathbb{P}(C_i) \log(1 + \theta_i)$, where C_i is the event that UE _{i} is in coverage. The sum throughput of the typical cell is thus $\mathcal{T}_1 + \mathcal{T}_2$. As BW_i is a function of both α and β , the resources to be allocated in a pNOMA setup for a given α are $P_1 = (1 - P_2)$, θ_1 , θ_2 and β .

C. SIRs Associated With pNOMA and Coverage Events

Because pNOMA uses FSIC, there are multiple SIRs of interest. For the two-user downlink pNOMA we require SIR_j^i , the SIR for decoding the j th message at UE _{i} where $i \leq j$ and the messages of all UEs weaker than UE _{j} have been removed while the messages of all UEs stronger than UE _{j} are treated as noise. In particular,

$$\text{SIR}_2^2 = \left(h_2 R_2^{-\eta} P_2 \right) / \left(h_2 R_2^{-\eta} P_1 \mathcal{I}(\alpha, \beta) + \tilde{I}_2^\circ \right) \quad (3)$$

$$\text{SIR}_1^2 = \left(h_1 R_1^{-\eta} P_2 \mathcal{I}(\alpha, \beta) \right) / \left(h_1 R_1^{-\eta} P_1 + \tilde{I}_1^\circ \right) \quad (4)$$

$$\text{SIR}_1^1 = \left(h_1 R_1^{-\eta} P_1 \right) / \tilde{I}_1^\circ \quad (5)$$

where \tilde{I}_i° is the ICI experienced at UE _{i} , $\tilde{I}_i^\circ = (P_i + (1 - P_i)\mathcal{I}(\alpha, \beta)) \sum_{\mathbf{x} \in \Phi} g_{\mathbf{y}_i} \|\mathbf{y}_i\|^{-\eta}$, where $\mathbf{y}_i = \mathbf{x} - \mathbf{u}_i$ and \mathbf{u}_i is the location of UE _{i} . The fading coefficient from the serving BS (interfering BS) located at \mathbf{o} (\mathbf{x}) to UE _{i} is h_i ($g_{\mathbf{y}_i}$). The ICI scaled to unit transmission power by each interferer is defined as I_i° , hence, $\tilde{I}_i^\circ = (P_i + (1 - P_i)\mathcal{I}(\alpha, \beta)) I_i^\circ$. Because $(P_i + (1 - P_i)\mathcal{I}(\alpha, \beta)) \leq 1$, ICI in pNOMA is lower than its traditional counterparts. Additionally, since the network model conditions an interferer to exist at a distance ρ from the typical BS at \mathbf{o} , we can rewrite I_i° as

$$I_i^\circ = \sum_{\mathbf{x} \in \Phi, \|\mathbf{x}\| > \rho} g_{\mathbf{y}_i} \|\mathbf{y}_i\|^{-\eta} + \sum_{\mathbf{x} \in \Phi, \|\mathbf{x}\| = \rho} g_{\mathbf{y}_i} \|\mathbf{y}_i\|^{-\eta}. \quad (6)$$

Note that as there is no interfering BS inside $b(\mathbf{o}, \rho)$, the nearest interfering BS from UE _{i} is at least $\rho - R_i$ away. As $\rho - R_i > R_i$, the in-disk model offers a larger guard zone than the usual guard zone of link distance for UEs in a downlink Poisson network [4].

While SIR_1^1 is associated with UE₁ decoding its message after decoding and cancelling the message of UE₂, FSIC also allows

UE₁ to decode its own message while treating the message of UE₂ as noise. The SIR associated with UE₁ for decoding its own message when the message of UE₂ has not been canceled is

$$\widetilde{\text{SIR}}_1^1 = (h_1 R_1^{-\eta} P_1) / (h_1 R_1^{-\eta} P_2 \mathcal{I}(\alpha, \beta) + \tilde{I}_1^0). \quad (7)$$

As FSIC decoding for UE₂ involves decoding its own message while treating the interference from the message of UE₁ as noise, the event of successful decoding at UE₂ is defined as

$$C_2 = \{\text{SIR}_2^2 > \theta_2\} = \{h_2 > R_2^\eta \tilde{I}_2^0 \bar{M}_2\}, \quad (8)$$

$$\bar{M}_2 = \theta_2 / (P_2 - \theta_2 P_1 \mathcal{I}(\alpha, \beta)). \quad (9)$$

FSIC decoding for UE₁, on the other hand, is the joint event as described in Section II-B. The event of successful decoding at UE₁ is thus defined as

$$\begin{aligned} C_1 &= \left\{ (\text{SIR}_2^2 > \theta_2 \cap \text{SIR}_1^1 > \theta_1) \cup \widetilde{\text{SIR}}_1^1 > \theta_1 \right\} \\ &= \left\{ h_1 > R_1^\eta \tilde{I}_1^0 M_1 \cup h_1 > R_1^\eta \tilde{I}_1^0 M_0 \right\} = \left\{ h_1 > R_1^\eta \tilde{I}_1^0 \bar{M}_1 \right\}, \end{aligned} \quad (10)$$

$$\begin{aligned} \bar{M}_1 &= \min\{M_0, M_1\} \mathbb{1}_{\tilde{P}_1 > 0} \mathbb{1}_{\tilde{P}_2 > 0} \mathbb{1}_{P_1 > 0} \\ &\quad + M_0 \mathbb{1}_{\tilde{P}_1 > 0} \mathbb{1}_{\tilde{P}_2 \leq 0} \cup P_1 \leq 0 + M_1 \mathbb{1}_{\tilde{P}_1 \leq 0} \mathbb{1}_{\tilde{P}_2 > 0} \mathbb{1}_{P_1 > 0} \end{aligned} \quad (11)$$

using $\tilde{P}_1 = P_1 - \theta_1 P_2 \mathcal{I}(\alpha, \beta)$, $\tilde{P}_2 = P_2 \mathcal{I}(\alpha, \beta) - \theta_2 P_1$, $M_0 = \theta_1 / \tilde{P}_1$ and $M_1 = \max\{\theta_2 / \tilde{P}_2, \theta_1 / P_1\}$.

The event of successful decoding at UE_i is thus of the form $C_i = \{h_i > R_i^\eta \tilde{I}_i^0 \bar{M}_i\}$. Using $\tilde{I}_i^0 = (P_i + (1 - P_i) \mathcal{I}(\alpha, \beta)) I_i^0$ and $\bar{M}_i = (P_i + (1 - P_i) \mathcal{I}(\alpha, \beta)) \tilde{M}_i$, we can rewrite C_i as

$$C_i = \{h_i > R_i^\eta I_i^0 \tilde{M}_i\}. \quad (12)$$

III. ANALYSIS OF THE META DISTRIBUTION

The CCP is defined as the coverage probability given a fixed network realization [12]. For a fixed, yet arbitrary, realization of the network \mathcal{P}_{C_i} , the CCP of UE_i in a pNOMA network is

$$\begin{aligned} \mathcal{P}_{C_i} &\triangleq \mathbb{P}(C_i | \Phi) \stackrel{(a)}{=} \mathbb{E}_{g_{\mathbf{y}_i}} \left[\exp(-R_i^\eta \tilde{M}_i \sum_{\mathbf{x} \in \Phi} g_{\mathbf{y}_i} \|\mathbf{y}_i\|^{-\eta}) | \Phi \right] \\ &\stackrel{(b)}{=} \prod_{\mathbf{x} \in \Phi} \left(1 + R_i^\eta \tilde{M}_i \|\mathbf{y}_i\|^{-\eta} \right)^{-1}, \end{aligned} \quad (13)$$

where (a) follows by using the definition of C_i in (12) and the cumulative distribution function (CDF) of $h_i \sim \exp(1)$. Using the moment generation function (MGF) of the independent random variables $g_{\mathbf{y}_i} \sim \exp(1)$, (b) is obtained.

The requirement for more fine-grained information on performance leads to the notion of studying the distribution of the CCP. The MD was thus defined as the CCDF of the CCP [12]. The MD for UE_i can be written as: $\bar{F}_{\mathcal{P}_{C_i}}(\mu) \triangleq \mathbb{P}(\mathcal{P}_{C_i} > \mu)$, $0 \leq \mu \leq 1$.

The b th moment of the CCP of UE_i, by definition, can be calculated using (13) as

$$\mathcal{M}_{i,b} = \mathbb{E}[\mathcal{P}_{C_i}^b] = \mathbb{E} \left[\prod_{\mathbf{x} \in \Phi} \left(1 + R_i^\eta \tilde{M}_i \|\mathbf{y}_i\|^{-\eta} \right)^{-b} \right]. \quad (14)$$

Note that by definition, the SCP of UE_i is the first moment of the CCP of UE_i, i.e., $\mathcal{M}_{i,1}$.

Deriving the MD is generally intractable. Therefore, the beta distribution using moment matching was proposed as a very accurate approximation for the MD [12]. This approach only requires the first two moments of the CCP, i.e., $\mathcal{M}_{i,1}$ and $\mathcal{M}_{i,2}$. In particular,

$$\bar{F}_{\mathcal{P}_{C_i}}(\mu) \approx 1 - \mathcal{I}_\mu \left(\beta_i \mathcal{M}_{i,1} (1 - \mathcal{M}_{i,1})^{-1}, \beta_i \right) \quad (15)$$

where $\beta_i = \frac{(\mathcal{M}_{i,1} - \mathcal{M}_{i,2})(1 - \mathcal{M}_{i,1})}{\mathcal{M}_{i,2} - \mathcal{M}_{i,1}^2}$ and $\mathcal{I}_\mu(a, b) = \int_0^\mu l^{a-1} (1-l)^{b-1} dl$ is the regularized incomplete beta function.

A. Exact Moments of the Conditional Coverage Probability

This subsection evaluates the moments of the CCP of UE_i.

Lemma 1: The b th moment of the CCP of UE_i is

$$\mathcal{M}_{i,b} \approx \mathbb{E}_{\rho, R_i} \left[\exp(-2\pi\lambda \mathcal{A}_{i,b}) \left(1 + \tilde{M}_i R_i^\eta \rho^{-\eta} \right)^{-b} \right], \quad (16)$$

$$\mathcal{A}_{i,b} = \int_{\rho - R_i}^\infty \left(1 - \left(1 + \tilde{M}_i R_i^\eta r^{-\eta} \right)^{-b} \right) r dr. \quad (17)$$

Proof: By writing $\mathcal{M}_{i,b}$ according to the definition in (14), and separating the ICI along the lines of (6), we obtain

$$\begin{aligned} \mathcal{M}_{i,b} &= \mathbb{E} \left[\prod_{\substack{\mathbf{x} \in \Phi \\ \|\mathbf{x}\| > \rho}} \left(1 + \tilde{M}_i R_i^\eta \|\mathbf{y}_i\|^{-\eta} \right)^{-b} \prod_{\substack{\mathbf{x} \in \Phi \\ \|\mathbf{x}\| = \rho}} \left(1 + \tilde{M}_i R_i^\eta \|\mathbf{y}_i\|^{-\eta} \right)^{-b} \right] \\ &\stackrel{(a)}{=} \mathbb{E}_{\rho, R_i} \left[e^{-2\pi\lambda \mathcal{A}_{i,b}} \mathbb{E}_w \left[\left(1 + \tilde{M}_i R_i^\eta w^{-\eta} \right)^{-b} \right] \right] \\ &\stackrel{(b)}{\approx} \mathbb{E}_{\rho, R_i} \left[e^{-2\pi\lambda \mathcal{A}_{i,b}} \left(1 + \tilde{M}_i R_i^\eta \mathbb{E}[w]^{-\eta} \right)^{-b} \right]. \end{aligned}$$

Using (6), the second term inside the expectation comes from the nearest interferer from \mathbf{o} which is a distance ρ from \mathbf{o} , while the first term comes from the other interferers that are located at distances larger than ρ from \mathbf{o} . In (a), we arrive at the first term of this expression and (16) using the probability generating functional (PGFL) of the PPP. Note that since the in-disk model allows a larger guard zone, the lower limit on the distance from the nearest interferer, in the inner integral $\mathcal{A}_{i,b}$, is $\rho - R_i$. The second term of (a) comes from denoting the distance between UE_i and the BS at distance ρ from \mathbf{o} by w . For simplicity, in (b) we used the approximate mean of the distance w which was validated as a tight approximation and in (16) $\mathbb{E}[w] \approx \rho$ as the difference between $\mathbb{E}[w]$ and ρ is less than 3.2% [4]. \square

For general b , $\mathcal{M}_{i,b}$ requires a triple integral according to (16). However, for $b \in \{1, 2\}$, closed-form expressions for $\mathcal{A}_{i,b}$ in (16) can be obtained, reducing the calculation in (16) by one integral. Note that $\mathcal{M}_{i,1}$ and $\mathcal{M}_{i,2}$ are the two most relevant moments of the CCP of UE_i, as they are sufficient to evaluate the MD of UE_i. **Corollary 1:** The inner integral for calculating the first moment of the CCP, i.e., the SCP, of UE_i, $\mathcal{M}_{i,1}$, is

$$\mathcal{A}_{i,1} = \frac{\tilde{M}_i R_i^\eta}{\eta - 2} (\rho - R_i)^{2-\eta} {}_2F_1 \left(1, 1 - \delta; 2 - \delta; \frac{-\tilde{M}_i R_i^\eta}{(\rho - R_i)^\eta} \right). \quad (18)$$

Corollary 2: The inner integral for calculating the second moment of the CCP of UE_i, $\mathcal{M}_{i,2}$, is

$$\begin{aligned} \mathcal{A}_{i,2} &= \frac{\tilde{M}_i R_i^\eta}{\eta} \left(\frac{2(\rho - R_i)^\eta + \tilde{M}_i R_i^\eta (\rho - R_i)^{2-\eta}}{(\rho - R_i)^\eta + \tilde{M}_i R_i^\eta} \right) \\ &\quad + \frac{(\eta - 2) \tilde{M}_i R_i^\eta}{2(1 - \eta)} (\rho - R_i)^{2-2\eta} {}_2F_1 \left(1, 2 - \delta; 3 - \delta; -\tilde{M}_i R_i^\eta (\rho - R_i)^{-\eta} \right) \\ &\quad + \frac{4(\rho - R_i)^{2-\eta}}{(\eta - 2)} {}_2F_1 \left(1, 1 - \delta; 2 - \delta; -\tilde{M}_i R_i^\eta (\rho - R_i)^{-\eta} \right). \end{aligned} \quad (19)$$

B. Approximate Moments of the Conditional Coverage Probability

Evaluating the b th moment of the CCP of UE_i in Section III-A requires a triple integral for general b , and a double integral for $b = 1, 2$. Therefore, an alternative approach to calculate the moments that is based on the relative distance process (RDP) is used [15]. Since pNOMA deals with ordered link distances, the ordered RDP is used, which for UE_i is defined as: $\mathcal{R}_i = \{\mathbf{x} \in \Phi : R_i \|\mathbf{y}_i\|^{-1}\}$.

Using the ordered RDP for UE_i, we can rewrite the moments of the CCP of UE_i in (14) as

$$\mathcal{M}_{i,b} = \mathbb{E} \left[\prod_{z \in \mathcal{R}_i} (1 + \tilde{M}_i z^\eta)^{-b} \right]. \quad (20)$$

As (14) is in terms of the PPP Φ , evaluating $\mathcal{M}_{i,b}$ in (16) requires the probability generating functional (PGFL) of the PPP. Accordingly, as $\mathcal{M}_{i,b}$ in (20) is in terms of the RDP \mathcal{R}_i , the PGFL of \mathcal{R}_i is required to evaluate $\mathcal{M}_{i,b}$. Because \mathcal{R}_i and therefore the RDP \mathcal{R}_i are conditioned on ρ , the PGFL of \mathcal{R}_i is also conditioned on ρ .

Lemma 2: The PGFL of the ordered \mathcal{R}_i conditioned on ρ is

$$\mathcal{G}_{\mathcal{R}_i|\rho}[f] = \mathbb{E}_{R_i|\rho} \left[\exp \left(-2\pi\lambda \int_{\rho-R_i}^{\infty} \left(1 - f \left(\frac{R_i}{a} \right) \right) a da \right) \prod_{\substack{\mathbf{x} \in \Phi \\ \|\mathbf{x}\| = \rho}} f \left(\frac{R_i}{\|\mathbf{y}_i\|} \right) \right]. \quad (21)$$

Proof: By definition of the PGFL we have

$$\mathcal{G}_{\mathcal{R}_i|\rho}[f] \triangleq \mathbb{E} \left[\prod_{z \in \mathcal{R}_i} f(z) \right] = \mathbb{E} \left[\prod_{\mathbf{x} \in \Phi} f(R_i \|\mathbf{y}_i\|^{-1}) \right].$$

By separating the interferers along the lines of (6) and using the PGFL of the PPP, (21) is obtained. \square

However, it is infeasible to obtain tractable expressions for the moments of the CCP using (21). Therefore, we propose the use of two approximations to relax the constraints and simplify the calculation of the PGFL of the ordered RDP for UE_i. The approximations are:

- **A1:** The guard zone around the UEs is approximated to be of radius R_i (instead of the largest guaranteed radius $\rho - R_i > R_i$).
- **A2:** Deconditioning on the BS located a distance ρ from \mathbf{o} .

Note that the two approximations have opposing effects on how much ICI is accounted; **A1** overestimates it while **A2** underestimates it.

Lemma 3: The PGFLs of the ordered RDP for UE₂ and UE₁, respectively, using approximations **A1** and **A2** are

$$\tilde{\mathcal{G}}_{\mathcal{R}_2|\rho}[f] = \frac{32 \Gamma(2) - \Gamma \left(2, \frac{\rho^2}{2} \pi \lambda \int_1^\infty \left(1 - f \left(\frac{1}{y} \right) \right) y dy \right)}{\rho^4 \left(2\pi\lambda \int_1^\infty \left(1 - f \left(\frac{1}{y} \right) \right) y dy \right)^2} \quad (22)$$

$$\tilde{\mathcal{G}}_{\mathcal{R}_1|\rho}[f] = \frac{\Gamma(1) - \Gamma \left(1, \frac{\rho^2}{2} \pi \lambda \int_1^\infty \left(1 - f \left(\frac{1}{y} \right) \right) y dy \right)}{\frac{\rho^2}{4} \pi \lambda \int_1^\infty \left(1 - f \left(\frac{1}{y} \right) \right) y dy} - \tilde{\mathcal{G}}_{\mathcal{R}_2|\rho}[f]. \quad (23)$$

Proof: Along the lines of the proof of Lemma 2, the PGFL of the ordered RDP for UE_i using **A1** and **A2** is

$$\tilde{\mathcal{G}}_{\mathcal{R}_i|\rho}[f] = \mathbb{E}_{R_i|\rho} \left[\exp \left(-2\pi\lambda \int_{R_i}^{\infty} (1 - f(R_i/a)) a da \right) \right].$$

Here the second term in (21) has been removed due to **A2**. Additionally, the lower limit of the integral of the first term in (21) is updated to reflect R_i , the radius of the guard zone in **A1**. Using $f_{R_i|\rho}$ in (2) for $i = 2$ and $i = 1$ we obtain (22) and (23), respectively. \square

Lemma 4: The b th moments of the CCP for UE₂ and UE₁, respectively, using approximations **A1** and **A2** are

$$\begin{aligned} \tilde{\mathcal{M}}_{2,b} &= \mathbb{E}_\rho \left[\frac{32 \Gamma(2) - \Gamma \left(2, \frac{\rho^2}{4} \pi \lambda \left({}_2F_1(b, -\delta; 1 - \delta; -\tilde{M}_2) - 1 \right) \right)}{\rho^4 \left(\pi \lambda \left({}_2F_1(b, -\delta; 1 - \delta; -\tilde{M}_2) - 1 \right) \right)^2} \right] \quad (24) \\ \tilde{\mathcal{M}}_{1,b} &= \mathbb{E}_\rho \left[\frac{8 \Gamma(1) - \exp \left(-\frac{\rho^2}{4} \pi \lambda \left({}_2F_1(b, -\delta; 1 - \delta; -\tilde{M}_1) - 1 \right) \right)}{\rho^2 \pi \lambda \left({}_2F_1(b, -\delta; 1 - \delta; -\tilde{M}_1) - 1 \right)} \right] \end{aligned}$$

$$\left. - \frac{32 \Gamma(2) - \Gamma \left(2, \frac{\rho^2}{4} \pi \lambda \left({}_2F_1(b, -\delta; 1 - \delta; -\tilde{M}_1) - 1 \right) \right)}{\rho^4 \left(\pi \lambda \left({}_2F_1(b, -\delta; 1 - \delta; -\tilde{M}_1) - 1 \right) \right)^2} \right]. \quad (25)$$

Proof: Using the definition in (20), we have

$$\tilde{\mathcal{M}}_{i,b} = \mathbb{E}_\rho \left[\tilde{\mathcal{G}}_{\mathcal{R}_i|\rho}[f(z)] \Big|_{f(z)=(1+\tilde{M}_i z^\eta)^{-b}} \right].$$

$\tilde{\mathcal{G}}_{\mathcal{R}_i|\rho}[f(z)]$ in (23) and (22) for UE₁ and UE₂, respectively, are then plugged into the equation above. We arrive at (24) and (25) using the following, where (a) is obtained using $z \rightarrow g^{-1}$:

$$\begin{aligned} & \int_1^\infty (1 - f(z^{-1})) z dz \Big|_{f(z)=(1+\tilde{M}_i z^\eta)^{-b}} \\ &= \int_1^\infty \left(1 - (1 + \tilde{M}_i z^{-\eta})^{-b} \right) z dz \stackrel{(a)}{=} \frac{{}_2F_1(b, -\delta; 1 - \delta, -\tilde{M}_i) - 1}{2}. \quad \square \end{aligned}$$

IV. RESULTS

We consider BS intensity $\lambda = 10$ and $\eta = 4$. Simulations are repeated 10^5 times. Fixed resource allocation (RA) is used in some of the figures while the other figures use the optimum RA associated with a problem that aims to maximize cell sum throughput while constrained to a threshold minimum throughput (TMT) according to [1, Algorithm 1]. Note that solving such a problem results in RA such that the minimum required resources are spent on UE₂ to attain throughput equal to the TMT and the remaining resources are given to UE₁ to maximize its throughput. The exact moments of the CCP are used unless specified otherwise.

Fig. 1 is a plot of the MD, using both the exact moments (Lemma 1) and the approximate moments (Lemma 4), for $\alpha = 0.3$ and $\alpha = 1$, traditional NOMA, using fixed RA. The figure validates the analysis in Section III as the simulation results are a tight match with the exact moments. The approximate moments are not as close to the simulation but follow the same trends which still gives insights on network performance at a lower computational cost. As anticipated, due to the opposing natures of **A1** and **A2**, the approximate moments can both underestimate and overestimate the MD. Focusing on the exact moments, we observe that for $\alpha = 0.3$, 93% of UE₁ and 78.2% of UE₂ achieve a reliability of 0.8. With $\alpha = 1$, on the other hand, only 81.9% of UE₁ and 47.7% of UE₂ achieve a reliability of 0.8. Thus, a notable improvement in the percentage of UEs able to achieve the same reliability is observed for both UEs (13.5% increase for UE₁ and 63.9% for UE₂) in pNOMA compared to NOMA. We also observe that the 5%-user performance that network operators are often interested in, defined as the reliability that 95% of the UEs achieve but 5% do not, has similar trends. With $\alpha = 0.3$, 95% of UE₁ (UE₂) achieve a reliability of 0.76 (0.58), while in NOMA, they achieve a reliability of 0.55 (0.245). These results emphasize the significance of the partial overlap on percentile performance.

Fig. 2 plots the MD for different α values using fixed RA. We observe that in general, when RA is fixed, increasing α deteriorates the performance of UE₂ due to the increasing $\mathcal{I}(\alpha, \beta)$ and consequently, interference. Thus the percentage of UE₂ that can achieve at least a certain coverage probability μ decreases with α . The performance of UE₁, on the other hand, is more complex as it first deteriorates as α increases from 0 to 0.5 and then improves from $\alpha = 0.5$ to 1. When $\alpha \leq 0.5$, UE₁ treats the message of UE₂ as noise; increasing α increases $\mathcal{I}(\alpha, \beta)$ and therefore

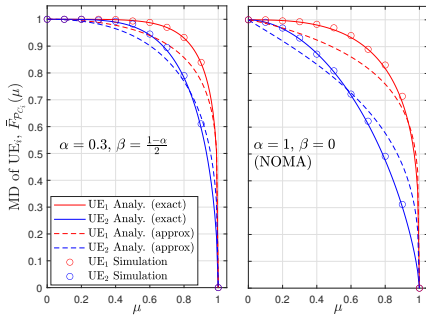


Fig. 1: MD vs. μ using $\theta_1 = 1$ dB, $\theta_2 = 0.5$ dB, and $P_1 = 1/3$.

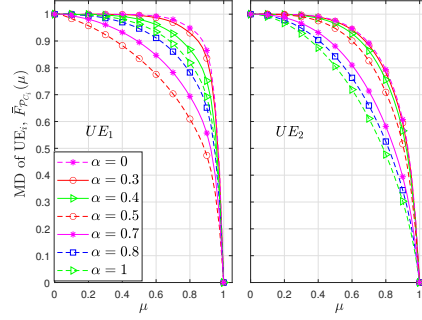


Fig. 2: MD vs. μ , $P_1=1/3$, $\theta_1 = 1$ dB, $\theta_2 = 0.5$ dB and $\beta = \frac{1-\alpha}{2}$.

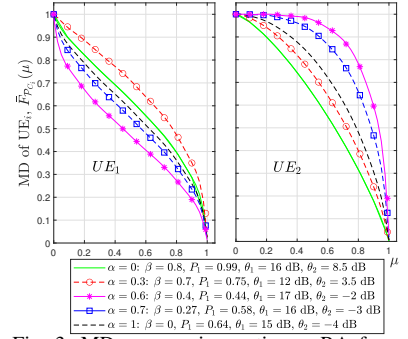


Fig. 3: MD vs. μ using optimum RA for each α with $TMT = 0.25$.

the IaCI from UE_2 , thereby deteriorating the performance of UE_1 . When $\alpha > 0.5$, there is a switch in decoding technique and the message of UE_2 is decoded by UE_1 before decoding its own message; increasing α and therefore $\mathcal{I}(\alpha, \beta)$ in this case increases the power of UE_2 's message making it easier to decode, thereby improving the performance of UE_1 . Thus, in Fig. 2, for UE_1 pNOMA outperforms NOMA ($\alpha = 1$) only when $\alpha \leq 0.4$, while for UE_2 pNOMA always outperforms NOMA.

Fig. 3 plots the MD for different α values using the optimum RA associated with $TMT = 0.25$. Unlike Fig. 2, the RA here is not the same for all α values and is specified in the legend for each α . The performance of UE_2 increases with α from 0 to 0.6. This occurs because increasing α increases BW_2 , lowering the θ_2 required to achieve $TMT = 0.25$. Increasing α beyond 0.6 decreases the performance of UE_2 as the dominance of the growing impact of $\mathcal{I}(\alpha, \beta)$ increases interference. While UE_2 aims to use the minimum resources to achieve TMT, the goal of UE_1 is to achieve the largest possible throughput. The performance in terms of the MD for UE_1 initially increases from $\alpha = 0$ to 0.3, as the increasing BW_1 reduces the θ_1 required to achieve maximum throughput. The performance decreases as α is increased to 0.6. This is attributed to the switch in decoding decoding at higher α . As $\mathcal{I}(\alpha, \beta)$ is not very high in this regime, decoding UE_2 's message is difficult for UE_1 , and thus UE_1 's performance suffers. Increasing α beyond 0.6 improves performance as the higher $\mathcal{I}(\alpha, \beta)$ makes decoding UE_2 's message easier for UE_1 and as the increasing BW for both UEs allows more power to be left for UE_1 's message.

We observe, from Figs. 1 and 2 explicitly, that UE_2 with the appropriate α outperforms its NOMA counterpart more than UE_1 . This can be attributed to the additional flexibility that comes with the ability to select α and β in pNOMA, which are fixed in NOMA. The observation sheds light on the fact that with appropriate α , pNOMA is able to assist the weaker UE significantly more than NOMA highlighting the role of pNOMA in improving UE fairness.

V. CONCLUSION

The MD of a pNOMA network was studied to obtain fine-grained information on network performance. Integral expressions were obtained for the moments of the CCP. We reduced the integrals for the first two moments, which are required for approximating the MD via moment matching. By proposing the use of two approximations, accurate approximate moments of the CCP were derived that further simplified the integral calculation.

We showed that in terms of percentile performance of links, pNOMA outperforms NOMA only when α is lower than a certain value. This highlights that deploying pNOMA over NOMA is only efficient when α is low and sheds light on careful parameter selection. Our results also indicated that pNOMA helps improve the performance of weaker UEs highlighting its significance as a means to improve UE fairness.

REFERENCES

- [1] K. S. Ali, E. Hossain, and M. J. Hossain, "Partial non-orthogonal multiple access (NOMA) in downlink Poisson networks," *IEEE Trans. Wireless Commun.*, vol. 19, no. 11, pp. 7637–7652, 2020.
- [2] B. Blaszczyzyn *et al.*, *Stochastic Geometry Analysis of Cellular Networks*. Cambridge University Press, 2018.
- [3] H. ElSawy *et al.*, "Modeling and analysis of cellular networks using stochastic geometry: A tutorial," *IEEE Commun. Surveys and Tutorials*, vol. 19, no. 1, pp. 167–203, Firstquarter 2017.
- [4] K. S. Ali, M. Haenggi, H. E. Sawy, A. Chaaban, and M. Alouini, "Downlink non-orthogonal multiple access (NOMA) in Poisson networks," *IEEE Trans. Commun.*, vol. 67, no. 2, pp. 1613–1628, Feb. 2019.
- [5] K. S. Ali, H. ElSawy, A. Chaaban, and M. S. Alouini, "Non-orthogonal multiple access for large-scale 5G networks: Interference aware design," *IEEE Access*, vol. 5, pp. 21 204–21 216, 2017.
- [6] H. Tabassum, E. Hossain, and M. J. Hossain, "Modeling and analysis of uplink non-orthogonal multiple access (NOMA) in large-scale cellular networks using poisson cluster processes," *IEEE Trans. Commun.*, vol. 65, no. 8, pp. 3555–3570, Aug. 2017.
- [7] Z. Zhang, H. Sun, and R. Q. Hu, "Downlink and uplink non-orthogonal multiple access in a dense wireless network," *IEEE J. Sel. Areas Commun.*, vol. 35, no. 12, pp. 2771–2784, Dec. 2017.
- [8] Z. Zhang, H. Sun, R. Q. Hu, and Y. Qian, "Stochastic geometry based performance study on 5G non-orthogonal multiple access scheme," in *Proc. of IEEE Global Commun. Conf.*, Dec. 2016, pp. 1–6.
- [9] K. S. Ali, H. E. Sawy, and M. Alouini, "Meta distribution of downlink non-orthogonal multiple access (NOMA) in Poisson networks," *IEEE Wireless Comm. Letters*, vol. 8, no. 2, pp. 572–575, Apr. 2019.
- [10] M. Salehi, H. Tabassum, and E. Hossain, "Meta distribution of SIR in large-scale uplink and downlink NOMA networks," *IEEE Transactions on Communications*, vol. 67, no. 4, pp. 3009–3025, 2019.
- [11] P. D. Mankar and H. S. Dhillon, "Meta distribution for downlink NOMA in cellular networks with 3GPP-inspired user ranking," in *2019 IEEE Global Communications Conf. (GLOBECOM)*, 2019, pp. 1–6.
- [12] M. Haenggi, "The meta distribution of the SIR in Poisson bipolar and cellular networks," *IEEE Trans. Wireless Commun.*, vol. 15, no. 4, pp. 2577–2589, Apr. 2016.
- [13] A. Alammouri *et al.*, "In-band α -duplex scheme for cellular networks: A stochastic geometry approach," *IEEE Trans. Wireless Commun.*, vol. 15, no. 10, pp. 6797–6812, Oct. 2016.
- [14] H. A. David, *Order statistics*. NJ: John Wiley, 1970.
- [15] R. K. Ganti and M. Haenggi, "Asymptotics and approximation of the SIR distribution in general cellular networks," *IEEE Trans. Wireless Commun.*, vol. 15, no. 3, pp. 2130–2143, Mar. 2016.